Latin American Journal of Solids and Structures
www.lajss.org

Three-Dimensional Finite Element Analysis of Compressive Behavior of Circular Steel Tube-Confined Concrete Stub Columns by New Confinement Relationships

Abstract

This paper presents a nonlinear analysis of axially loaded steel tube-confined concrete (STCC) stub columns with new confinement relationships. For this aim, a 3-D finite element model of STCC columns using ABAQUS program is developed and validated against the experimental data. Proper material constitutive models are proposed and the confinement parameters of confined concrete are determined by matching the numerical results via trial and error. The parameters considered for quantitative verification of the FE model include five different factors indicating the behavior of STCC columns: compressive strength corresponding to steel yielding point, initial peak strength and ultimate strength as well as longitudinal to circumferential stress ratio of steel tube at steel yielding point and initial peak point. For the qualitative verification, the axial and lateral stress–strain relationships of STCC columns are taken into account. The comparison results indicate that the model can accurately predict the compressive behavior of STCC stub columns. Finally, a parametric study is also performed to evaluate the effect of tube diameter-to-wall thickness ratio (D/t), concrete compressive strength (f_c) and steel yield strength (f_y) on the compressive behavior of STCC columns. According to the results of the parametric study, the interface shear stress and lateral confining pressure are not affected by f_c while significantly increase with decreasing D/t.

Keywords

Confined concrete; Finite element analysis; Stub column; Confinement relationships; Compressive strength; Axial compression.

Akbar Haghinejad
Mahdi Nematzadeh *

Department of Civil Engineering, University of Mazandaran, 47416-13534, Babolsar, Iran

* Corresponding author
email:m.nematzadeh@umz.ac.ir,
Tel. +98 9111146772;
fax: +98 1135302903.

http://dx.doi.org/10.1590/1679-78252631

Received 19.11.2015
In revised form 13.01.2016
Accepted 11.02.2016
Available online 17.02.2016

1 INTRODUCTION

Concrete confinement creates a triaxial stress, which increases concrete strength and ductility (Bahrami et al. 2013; Han et al. 2005; Bahrami et al. 2014). In recent years, the use of steel tube-

confined concrete (STCC) columns in modern structures has been the field of interest for many structural engineers. In these columns, the load is only applied on the concrete core. Hence, the role of steel tube in concrete confinement is more effective. Moreover, because of small compressive axial load carried by the confining tube in STCC columns, the possibility of local buckling of the steel tube decreases significantly (Wang et al. 2011; Aboutaha and Machado 1998). In addition, the steel tube in STCC columns is used as permanent formworks, leading to no need for concrete shuttering and curing and consequently reduction in the construction time and cost.

So far, much experimental research has been carried out to investigate the performance of STCC columns. It seems that Tomii et al. (1985) conducted the first studies on the behavior of STCC columns. They improved the ductility of reinforced concrete stub columns through confining them by steel tubes and used it as a method to prevent shear failures. Experimental investigation of Han et al. (2005) illustrated that STCC columns exhibit high levels of ductility and energy dissipation, especially when they are under high axial loads. Aboutaha and Machado (1998) studied the behavior of STCC columns and compared the obtained results with those of concrete filled-steel tube (CFST) columns. They found that effective confinement of concrete core increases and the possibility of steel tube buckling decreases in STCC columns more than CFST ones. One of the latest experimental researches on STCC columns has been performed by Nematzadeh (2012) in which portion of steel tube confinement is separated from its axial load carrying portion. Their results showed that the confinement effectiveness coefficient of STCCs is about half that of the experimental results of Richart et al. (1928).

There is little research available in the literature on developing an exact model for simulating the concrete confinement in STCC columns. Using the ABAQUS program, Schneider (1998) presented a 3-D nonlinear finite element model for CFST columns. To define the properties of concrete material in this model, the stress-strain curve of unconfined concrete was used in the absence of the strain hardening for steel material. His results showed that the finite element model can predict the elastic and inelastic behavior of the columns precisely. Hu et al. (2003) used a confined concrete stress-strain curve to define the properties of concrete material and a bilinear stress-strain curve for steel material in ABAQUS program. They verified the results obtained from the model with the experimental results of Schneider (1998) and Huang et al. (2002). From the results of numerical simulations, they also presented empirical equations of the lateral confining pressure applied to the concrete core. Ellobody et al. (2006) used a confined concrete stress-strain and a multi linear stress-strain curve for concrete and steel material, respectively, and studied the effect of concrete strength and cross-section geometries on the compressive behavior of circular CFST columns. Wang et al. (2011) investigated the numerical behavior of STCC columns in their research. Their results indicated that in STCC columns due to small compressive axial load carried by the steel tube, the eftiveness of the tube in confining the concrete core is high and its local buckling possibility is low. Hence, thinner steel tube can be utilized in STCC columns compared with the CFST ones. Gupta and Singh (2014) investigated the numerical behavior of short concrete filled steel tubular (CFST) columns by providing a 3-D finite element program and verifying the proposed model through comparison with the corresponding experimental specimens. It is observed that the value of radial confining pressure in the area adjacent to top and bottom platens is markedly higher than the value in-between due to the end restraint provided by the machine platens. Yu et al. (2010) by using the

experimental results of Han et al. (2005) developed a 3-D finite element model and evaluated the behavior of STCC columns under axial compression load. In order to define the concrete material in the model, the stress-strain curve similar to that of CFST columns was used. Their results showed that load-carrying capacity of circular STCC columns is more than the CFST ones.

Despite that STCC columns are widely used in engineering structures and exhibit a good performance, there is not enough information available in the literature regarding their analysis. This paper presents a nonlinear analysis on the behavior of circular STCC stub columns under axial compression load along with confinement effect. For this purpose, an appropriate 3-D finite element model is developed using ABAQUS (ABAQUS 6.12, 2012) program to be verified against the experimental results of STCC columns conducted by Nematzadeh (2012). Appropriate equations are presented for the concrete confinement parameters, by matching the finite element (FE) results with the experimental data via trial and error. The parameters considered for quantitative verification of the FE model include the compressive strength corresponding to the yield, initial peak and ultimate point of steel and ratio of longitudinal to hoop stress of steel tube at the yield and initial peak point of steel. Furthermore, both the axial and lateral stress–strain relationships of STCC columns are considered for quality validation. In order to define the concrete behavior in finite element model, the equivalent uniaxial stress-strain curve of confined concrete is used, in which the confinement effectiveness coefficient obtained from the experimental results of Nematzadeh (2012) is applied. Multi linear stress-strain curve is used for steel material. A parametric study is also performed and the effect of various parameters including tube diameter-to-wall thickness ratio, concrete compressive strength and steel yield stress on compressive behavior of STCC columns is evaluated.

2 FINITE ELEMENT MODELING

Modeling the behavior of steel tube-confined concrete (STCC) columns is performed in three main parts including confined concrete, confining steel tube and interaction between concrete core and steel tube. In addition, in finite element analysis of these columns, selection of element type and mesh size should be appropriate for accurate simulation of the behavior of the columns in a reasonable computational time. Since STCC columns under axial load are completely symmetrical, just 1/8 of the specimen is needed to model which leads to a significant reduction in computational time.

2.1 Element Type and Mesh

Various elements were used for simulation of STCC columns behavior and finally according to the results, steel tube and concrete core were modeled using 3-D solid element (C3D8R) available in ABAQUS program library. This element has eight nodes and each one has three translational degrees of freedom. Also, structured mesh is applied to simulate the confined columns. A pattern of the model in program is showed in Fig. 1. As shown in the figure, there is a height difference between top surfaces of concrete core and steel tube which is due to matching with experimental conditions of STCC specimens for applying the load on the concrete core only.

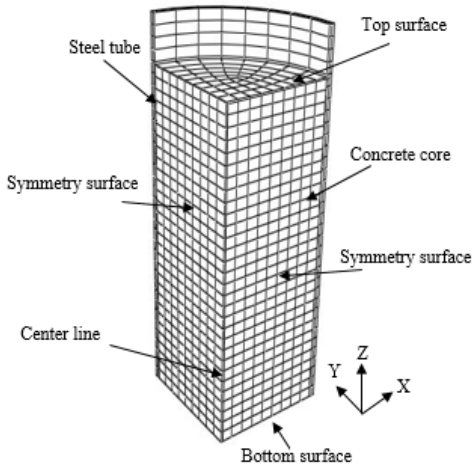

Figure 1: Finite element mesh of steel tube-confined concrete.

2.2 Boundary Condition and Load Application

To simulate the boundary condition of STCC specimens in the model, top surface of concrete core is restrained in all degrees of freedom except in loading direction while upper surface of steel tube is completely free. Also, bottom surface of the composite column including concrete and steel is free in all direction except in the loading direction. Lateral displacement of cut surfaces (XZ and YZ surfaces) in direction perpendicular to the surface is prevented because of the symmetry so that the center line has no movement in both X and Y directions. In the laboratory, solid steel plates were used for applying the axial load on end surfaces of concrete core (Nematzadeh, 2012), but in modeling, the results of this condition are similar to the case without the loading plates.

The axial load is applied on top surface of the concrete core equally in all surface nodes through strategy of displacement control in appropriate intervals via *STATIC GENERAL METHOD available in ABAQUS program library.

2.3 Modeling of Steel Tube Material

According to Fig. 2, a trilinear stress-strain curve is used to define the steel material behavior in ABAQUS program which includes three stages: elastic, yield and strain hardening. Main parameters for defining the stress-strain curve of steel include yield stress (f_y), ultimate stress (f_{su}), yield strain (ε_y), strain at the beginning of strain hardening (ε_p) and ultimate strain (ε_{su}), the values of which are presented in Table 1, based on the experimental results of (Nematzadeh, 2012). First part of steel stress-strain curve represents the elastic behavior of steel material which can be defined using *ELASTIC option in ABAQUS program library where Young's modulus and Poisson's ratio are considered equal to 210 GPa and 0.28, respectively. Also, *PLASTIC option in the program library is used to introduce the inelastic behavior of steel material including yield and strain hardening stages.

Since the steel tubes used in experiments are seamless hot-rolled (Nematzadeh, 2012), they have no residual stresses caused by the welding process. von Mises criterion, known as the maximum distortion energy criterion or octahedral shear stress theory, is used in this study to estimate the steel yield stress. Although the Tresca criterion known as the maximum shear stress criterion is generally easier to apply in comparison with the von Mises criterion, the latter is in better agreement with the actual response of most metals. The Tresca criterion usually gives conservative results in prediction of the system strength (Leckie and Bello 2009).

f_y (MPa)	f_{su} (MPa)	ε_y	ε_p	ε_{su}
339	480	0.0016	0.0139	0.114

Table 1: Mechanical properties of steel tube (Nematzadeh, 2012).

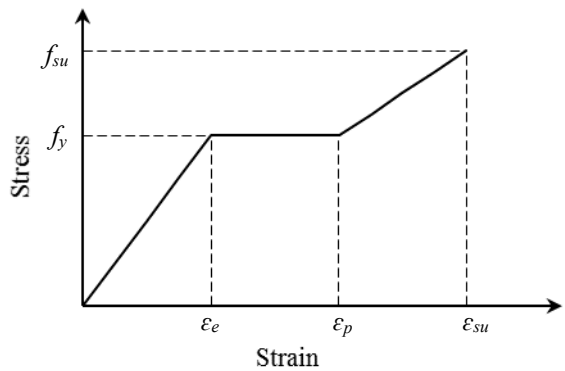

Figure 2: Equivalent stress-strain curve of steel.

2.4 Modeling of Confined Concrete Material

2.4.1 Concrete Stress-Strain Curve

Since ABAQUS program is able to consider the confinement effect in improving the behavior of the confined concrete by using models such as Drucker-Prager, it seems that unconfined concrete behavior should be used to define the concrete material in ABAQUS. In this field, Schneider (2003) conducted an analytical study on compressive behavior of CFST columns, in which the unconfined uniaxial stress-strain curve is used to define the concrete material in the ABAQUS. Nevertheless, many researchers have applied the confined concrete model in the program to define the compressive behavior of concrete (Hu et al. 2003; Ellobody et al. 2006; Yu et al. 2010). One of the main reasons for this fact is the lack of real modeling of confinement and the increased strength caused by it in ABAQUS program especially in high confinement values. This is because there are various parameters in the program to define the inelastic stage of concrete material, based on which the empirical uniaxial stress-strain curve of concrete is introduced. In this case, Hu et al. (2003) presented empirical equations for the confinement levels of confined concrete for the definition of concrete material in the program using the trial and error method and matching the analytical results obtained from the ABAQUS with the experimental results of CFST columns.

In the present study, the results obtained from the analytical model of STCC specimens by using the unconfined behavior of concrete material, exhibit a significant difference with the experimental results so that this difference increases with increasing the confinement level. Hence, the confined uniaxial stress-strain curve is applied to define the concrete material in STCC model, the characteristics of which are a function of confinement level. Using various confinement levels for definition of concrete behavior in ABAQUS program and matching the obtained results with the experimental ones, empirical equations are achieved for the concrete confinement value in STCC columns, which are presented later. It should be noted that in general, the confinement level defined for the concrete material in STCC model is much smaller than the real confinement provided by the steel tube.

The equivalent uniaxial stress-strain curve presented in this study to define concrete behavior in ABAQUS program is shown in Fig. 3. The curve consists of three stages: linear stage, nonlinear stage for pre-peak and bilinear stage for post-peak. The first stage of the curve is linear with slope of E_{cc} known as modulus of elasticity of confined concrete. This stage of the curve continues to half the compressive strength of confined concrete ($0.5f_{cc}$) (Hu et al. 2003). It should be noted that a discontinuity is created in the stress-strain curve at the intersection between the linear stage and the nonlinear stage after that. The number of data points for definition of the concrete stress-strain curve must be enough so that no discontinuity would be created with negative slope at intersection of the first and second stage of the curve. In this condition, a discontinuity with positive slope is created in curve, which has a negligible effect on the FE results.

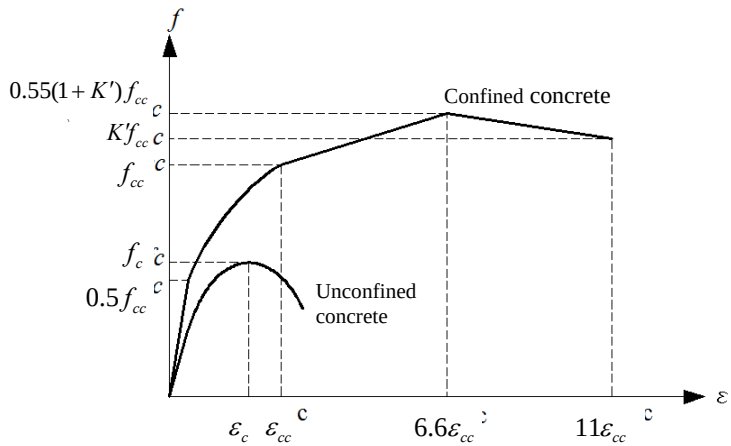

Figure 3: Equivalent uniaxial stress-strain curves of confined and unconfined concrete.

Modulus of elasticity of confined concrete is calculated from the relationship proposed by ACI 318 (2008) as follows

$$E_{cc} = 4730\sqrt{f_{cc}} \tag{1}$$

where E_{cc} and f_{cc} are modulus of elasticity and compressive strength of confined concrete in MPa, respectively. The value of f_{cc} can be obtained from Eq. (2) proposed by Richart et al. (1928) who

conducted the tests on the concrete confined with fluid pressure. In Eq. (2), k is confinement effectiveness coefficient and f_c and f_l are compressive strength of the unconfined concrete and lateral confining pressure, respectively. Strain corresponding to f_{cc}, ε_{cc} can be determine by Eq. (3) proposed by Mander et al. (1988), based on the experimental results of Richart et al.

$$f_{cc} = f_c + k\, f_l \tag{2}$$

$$\varepsilon_{cc} = \varepsilon_c \left(1 + 5k \frac{f_l}{f_c} \right) \tag{3}$$

where ε_c is strain of the unconfined concrete corresponding to f_c and is considered 0.003. According to the equations proposed by Nematzadeh (2012) for STCC columns, the parameter k is considered as a constant value equal to 2.17. However, a larger value is obtained by Richart et al., which is equal to 4.1. Due to the existence of the longitudinal compressive stress of steel tube in STCC columns, the confinement effect and thus the confinement effectiveness coefficient is reduced compared with the case without the longitudinal stress. The parameter f_l can be calculated by the trial and error method and matching the FE results with the experimental data, as follows

$$\frac{f_l}{f_y} = 0.034366 - 0.000452 \left(\frac{D}{t} \right) \tag{4}$$

The above equation indicates that the parameter f_l is independent of the concrete compressive strength. The relationship between f_l / f_y obtained from the matching and D/t (external diameter-to-wall thickness ratio of steel tube) is illustrated in Fig. 4. Since in Eqs. (2) and (3), the parameters k and f_l are multiplied together, it is possible to increase the value of k to 4.1 (proposed by Richart et al.) and in contrast, f_l is reduced by a linear reduction factor of 0.53.

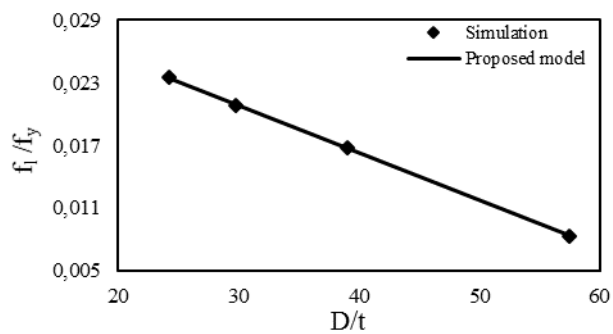

Figure 4: f_l / f_y obtained from matching results versus D/t of STCC columns.

The second stage of the stress-strain curve of confined concrete is nonlinear and is determined from Eq. (5) proposed by Saenz (1964), which starts at the end of linear stage and continues to f_{cc}.

$$f = \frac{E_{cc}\varepsilon}{1+(R+R_E-2)\left(\frac{\varepsilon}{\varepsilon_{cc}}\right)-(2R-1)\left(\frac{\varepsilon}{\varepsilon_{cc}}\right)^2+R\left(\frac{\varepsilon}{\varepsilon_{cc}}\right)^3} \tag{5}$$

where f and ε are uniaxial stress and strain of confined concrete, respectively. Also, R_E and R are modular ratio and ratio relation, respectively, and are obtained by the following equations.

$$R_E = \frac{E_{cc}\varepsilon_{cc}}{f_{cc}} \tag{6}$$

$$R = \frac{R_E(R_\sigma - 1)}{(R_\varepsilon - 1)^2} - \frac{1}{R_\varepsilon} \tag{7}$$

Constants R_ε and R_σ are strain ratio and stress ratio, respectively, which determine the stress-strain curve shape of concrete after peak point (descending branch). They are taken as 4.0 as recommended by Hu and Schnobrich (1989). Since these two parameters influence the ascending branch of the concrete stress-strain curve, they are can be used to define the second stage of the confined concrete stress-strain curve.

The third stage of the confined concrete stress-strain curve is bilinear. This stage starts at ε_{cc} and ended at strain equal to $11\varepsilon_{cc}$. The final stress is equal to $K'f_{cc}$ where, K' is the product of the two parameters K_c' and K_s' which are related to the compressive strength of unconfined concrete and the tube outer diameter-to-wall thickness ratio, respectively. By matching the FE results to the experimental stress-strain curve of STCC specimens, parameter K' is obtained as Eqs. (8a) and (8b), the value of which can be higher or lower than 1. It can be found from these equations that the value of K_c' and consequently K' decreases with increasing the concrete compressive strength because of the reduction in concrete ductility. Also, the increase in D/t leads to the decrease in the confining pressure and as a result the reduction in ductility of the confined concrete and thus reduction of K_s' and K'. Fig. 5 shows the curves of K_s' and K_c' versus D/t and f_c, respectively.

$$K' = K_s'K_c' = \left(0.0264865 - 0.0003861\frac{D}{t}\right)(85 - 0.625f_c)$$
$$24.2 \le \frac{D}{t} \le 29.75, \quad 16.7 \le f_c \le 52.6 \tag{8a}$$
$$24.2 \le \frac{D}{t} \le 29.75, \quad 16.7 \le f_c \le 52.6$$

$$K' = K_s'K_c' = \left(0.0169283 - 0.0000662\frac{D}{t}\right)(85 - 0.625f_c)$$
$$29.75 \le \frac{D}{t} \le 57.5, \quad 16.7 \le f_c \le 52.6 \tag{8b}$$

Stress and strain at the intersection between two lines of the third stage is considered 1.1 times higher than the average value of stress and strain between the endpoint of the second stage and the

endpoint of the third stage. Therefore, the stress and strain in the middle of the third stage are obtained equal to $0.55(K'+1)f_{cc}$ and $6.6\varepsilon_{cc}$, respectively. As mentioned for the steel stress-strain curve, it should be noted that the end point of the third stage in the confined concrete stress-strain curve does not imply the failure point, but the ABAQUS program considers a constant stress condition after endpoint.

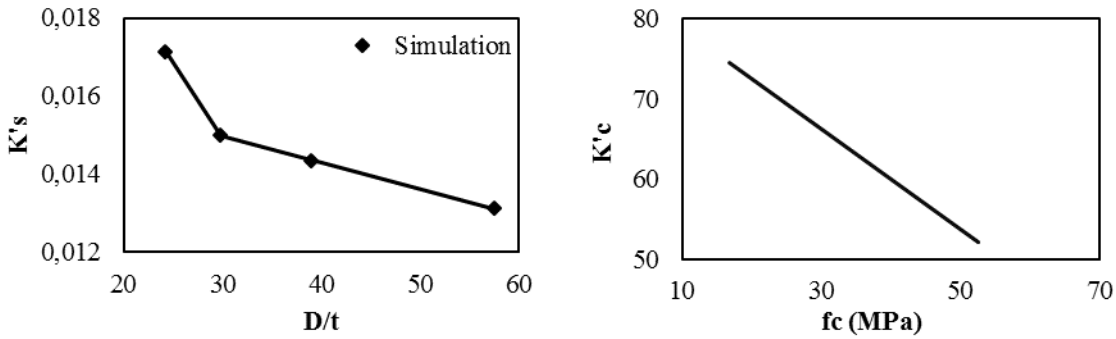

Figure 5: Relationship of K_s' and K_c' versus D/t and f_c for STCC columns.

Since the behavior of the confined concrete is used in the modeling, the plastic strain must be defined in the program as follows

$$\varepsilon^p = \varepsilon - \frac{f}{E_{cc}} + 2\nu_{cc}\frac{f_l}{E_{cc}} \tag{9}$$

where ε and f are uniaxial strain and stress of the confined concrete, respectively, obtained from Fig. 3. Also, ε^p is plastic strain and ν_{cc} is Poisson's ratio of the confined concrete which is considered equal to 0.2. In Eq. (9) and other equations of this research, the sign of compressive stress and strain is defined to be positive.

2.4.2 Yield Surface of Concrete

Since the concrete core in STCC columns is under triaxial compression, compressive yield surface of concrete increases with increasing the hydrostatic pressure. Drucker-Prager model (Chen and Saleeb 1994) can be used as one of the yield criteria of concrete, in which the concrete shear strength is expressed based on the hydrostatic pressure. Also, by considering a linear relationship between the shear strength and the confining pressure of concrete, the linear Drucker-Prager can be used for the concrete yield surface as Eq. (10).

$$F = q - p\tan\beta - d = 0 \tag{10}$$

where β is the friction angle of the material and d is the cohesion of the material. Also, p and q are equivalent pressure stress and Mises equivalent stress, respectively, which are defined in terms of the first stress invariant (I_1) and the second deviatoric stress invariant (J_2) as follows

$$p = \frac{I_1}{3}, \quad I_1 = \sigma_1 + \sigma_2 + \sigma_3 \tag{11}$$

$$q = \sqrt{3J_2}, \quad J_2 = \frac{1}{6}[(\sigma_1 - \sigma_2)^2 + (\sigma_3 - \sigma_2)^2 + (\sigma_3 - \sigma_1)^2] \tag{12}$$

where σ_1, σ_2 and σ_3 are principal stresses.

In ABAQUS, a modified yield criterion is used for concrete material which is a D-P type plasticity model, referred to the extended Drucker-Prager model. In this model, an additional parameter known as the flow stress ratio is adopted. This parameter controls the dependence of the yield surface on the value of the intermediate principal stress and is physically defined as the ratio of the yield stress in triaxial tension to that in triaxial compression, equal to the shear strength ratio of concrete under equal biaxial compression to that under triaxial compression.

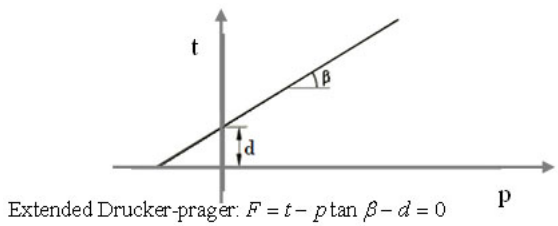

(a) Yield surface in the meridional plane (p-t).

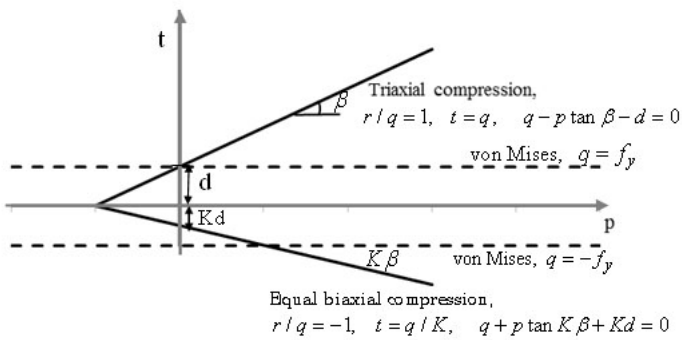

(b) Yield surface in the meridional plane (p-q) for a given K (0.778<K<1).

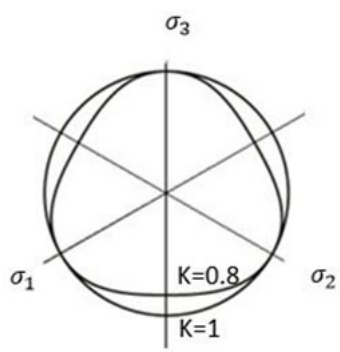

(c) Yield surface in the deviatoric plane for K=1 and K=0.8.

Figure 6: Extended linear Dracker-Prager yield surface.

Fig. 6a illustrates the extended Drucker-Prager yield surface which is compared with von Mises yield surface. According to this figure, the yield surface function (F) of the extended Drucker-Prager model is expressed as Eq. (13) in which t is replaced by q in Eq. (10).

$$F = t - p\tan\beta - d = 0 \tag{13}$$

where $t = \frac{1}{2}q\left[1 + \frac{1}{K} + \left(1 - \frac{1}{K}\right)\left(\frac{r}{q}\right)^3\right]$ is shear strength, in which K is shear strength ratio and r is defined in terms of the third invariant of deviatoric stress (J_3), as following equation:

$$r = 3\sqrt[3]{J_3/2}, J_3 = (\sigma_1 - p)(\sigma_2 - p)(\sigma_3 - p) \tag{14}$$

Fig. 6b shows the shape of the yield surface in meridional plane for a certain value of K. This figure indicates that two elements with the same material and the same hydrostatic pressure (p) can exhibit different yield strengths (q). It can also be seen that for $r/q = 1$ corresponding to the triaxial pressure condition, the equation $t = q$ is obtained that is the same as Eq. (10) for the conventional Drucker-Prager. Also, for $r/q = -1$ which corresponds to the equal biaxial pressure condition, the equation $t = q/K$ is achieved and the yield surface can be written as Eq. (15) where the friction angle and the cohesion of the material are K times those in the triaxial pressure condition.

$$F = t + p\tan K\beta + Kd = 0 \tag{15}$$

In the case of concrete material which has the hardening and softening behavior, the yield surface is not constant and changes parallel to the initial yield surface so that only the interception point (d) is different. Hence, the initial and final failure surfaces correspond to the beginning of the concrete nonlinear stage and the concrete failure, respectively.

Fig. 6c indicates the yield surface in the deviatoric plane for the two cases of $K = 1$ and $K = 0.8$. It can be seen from the figure that in the case of the former, the shape of yield surface is circular and yield stress for various r/q is the same and equal to q (similar to the conventional Drucker-Prager model). In the case of the later, the shape of yield surface is not circular and yield stress for various r/q is different (similar to the extended Drucker-Prager model). In order to make sure that the yield surface remains convex, it is necessary to apply the condition of $0.778 \le K \le 1.0$.

In circular STCC columns, the lateral stresses applied on the concrete core in different directions are the same, as shown in Fig. 7, and thus the stress parameters of Drucker-Prager model in the confined concrete can be summarized as Eqs. (16)-(18).

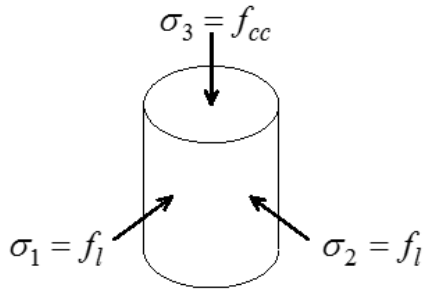

Figure 7: Stress condition of confined concrete in circular STC.

$$p = \frac{1}{3}(f_{cc} + 2f_l) \tag{16}$$

$$q = f_{cc} - f_l \tag{17}$$

$$r = f_{cc} - f_l \tag{18}$$

It should be noted that in this study Eqs. (16)–(18) are true at the mid-height of the STCC specimens because the friction at the interface between concrete core and steel tube makes a shear stress in the longitudinal direction, which changes the principal stresses condition indicated in Fig. 7. Using Eqs. (16)–(18), shear strength ratio (K) is obtained as 0.846 (see Appendix A), which in this research is considered to be 0.8 for the modeling of STCC specimens in ABAQUS. The results obtained from the FE model of STCC columns indicate that the compressive behavior of these columns exhibits little sensitivity to the K parameter. This fact can be clearly observed in Fig. 8. The reason for this is that according to Eqs. (16)–(18), r is equal to q ($r / q = 1$) and hence in the shear strength equation, t will be equal to q and independent of the parameter K.

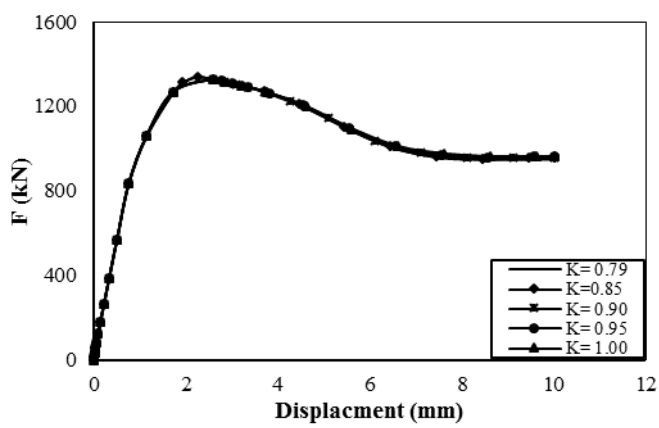

Figure 8: Parameter study of flow stress ratio (axial load-displacement curves of STCC for different values of K).

The friction angle β is defined for shear failure and it is the slope of the linear Dracker-Prager yield surface in the meridional plane geometrically. To apply the yield surface for the case of uniaxial compression, the condition of $\beta \leq 71.5^{\circ}$ must be established. This parameter can be calculated based on the triaxial and uniaxial compressive tests. In the present study, using the confinement relationship proposed in the previous article (Nematzadeh, 2012) for STCC columns, the friction angle of concrete material is obtained to be 40° (see Appendix B). It should be noted that the improved behavior of concrete material is used for the modeling in ABAQUS program so that its compressive strength and stress-strain curve are not in accordance with the experimental results of unconfined concrete, but are a function of the lateral confining pressure. For this reason, the friction angle achieved by the calculations leads to a poor agreement between the analytical and the experimental results. Hence, by matching the FE results via trial and error method for all the confined specimens, the friction angle is obtained to be 20°.

The cohesion parameter d is geometrically the intercept of the linear yield surface, and is related to the yield stress of the uniaxial compression as:

$$d = (1 - \frac{\tan\beta}{3}) f_c \tag{19}$$

For the STCC specimens, the parameter d is obtained to be 0.88. To determine the plastic deformation of the material, the flow potential (G) is defined for the linear Drucker-Prager model as follows

$$G = t - p\tan\psi \tag{20}$$

where ψ is the volumetric dilation angle which is a major parameter affecting the behavior of the material that governs the D-P flow rule and is used as a material parameter in ABAQUS. Physically, the dilation angle is defined as the ratio of plastic volume change to plastic shear strain and geometrically, it is the slope of the potential function in the p–t plane, as shown in Fig. 9. According this figure, If $\psi > 0$ the material dilates; if $\psi < 0$ the material contracts and if $\psi = 0$ the inelastic deformation is incompressible. To apply the flow potential for the case of uniaxial compression, the condition of $\psi < 71.5^{\circ}$ must be established that is likely for real material. Also, associated flow potential is referred to the case of $\psi = \beta$ and non-associated one is referred to the case of $\psi \neq \beta$ in which the flow potential is different from the yield function. The flow rule determines the direction of plastic deformation and relates G to the incremental plastic strain ($d\varepsilon^{p}$), defined as:

$$d\varepsilon_{ij}^{p} = \lambda \frac{\partial G}{\partial \sigma_{ij}} \tag{21}$$

where λ is a scalar hardening parameter which may vary throughout the straining process. Also, σ_{ij} is the components of principal stress including σ_1, σ_2 and σ_3 in radial, circumferential and longitudinal directions, respectively.

In this research, a non-associated flow rule is used to define the direction of the plastic flow. The dilation angle of confined concrete is obtained to be about 35° which is higher than the friction

angle while the dilation angle is usually lower than the friction angle. The results of this study indicate that for the case of $\psi \leq \beta$, although the axial stress-strain relationship obtained from the FE analysis is in a good agreement with the experimental results, there is a significant difference between their longitudinal to circumferential stress ratio of the steel tube in the plastic strains. The increase of ψ up to the values higher than β, although insignificantly affects the compressive strength and the shape of stress-strain curve of STCC columns, as shown in Fig. 10, considerably decreases the longitudinal to circumferential stress ratio of the steel tube at the steel yielding point and particularly at the strain hardening point. A parametric study of the dilation angle conducted in this study on the compressive behavior of the confined concrete indicates that the best agreement with the experimental results is reached for a dilation angle between 20° and 40°. It should be noted that low values of the dilation angle produce a brittle behavior while higher values make more ductile behavior. Moreover, a higher level of confinement is resulted in a more ductile behavior and consequently a higher value of the dilation angle. Hence, due to the high ductile of the confined concrete in STCC columns, a high value of the dilation angle is predictable. The flow potential eccentricity is considered 0.1 in ABAQUS.

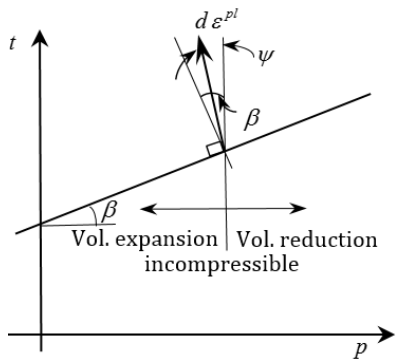

Figure 9: Plastic flow and volumetric behavior.

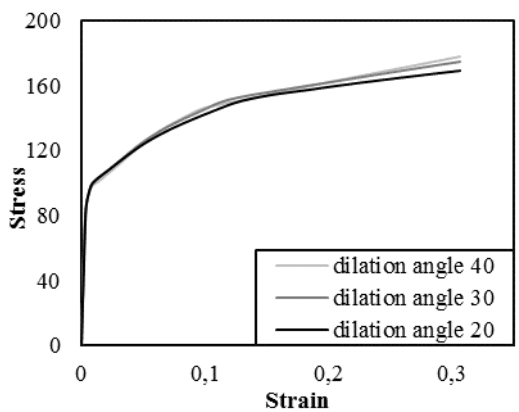

Figure 10: Parameter study of dilation angle with friction angle of 10 (axial stress-strain curves of STCC for different values of ψ).

2.5 Concrete-Steel Tube Interface Modeling

The contact between the steel tube and concrete core is modeled by the interface element which matches the faces of steel and concrete elements. Using normal behavior and choosing the hard contact interface available in the ABAQUS material library, the two contact elements are not allowed to penetrate each other. Also, the interface element allows the contact surfaces to separate under a tensile force. The friction at interface maintains until two faces remain in contact.

By matching the FE results by trial and error, the friction coefficient is obtained to be 0.65. Also, by conducting a parametric study, it is found that with increasing the friction coefficient, the longitudinal to hoop stress ratio of the steel tube increases at the yield and strain hardening points.

2.6 Failure Criterion

Since, the failure of all specimens is due to the rupture of steel tube at mid-height, the shear damage is selected in ABAQUS to cut the compressive stress-strain curve of STCC columns. The Shear damage criterion is a model for predicting the onset of damage due to shear band localization and is used for ductile metal. The shear criterion can be used in conjunction with the Mises. The model assumes that the equivalent plastic strain at the onset of damage is a function of the shear stress ratio and strain rate. The damage parameters in this model are fracture strain which is equivalent fracture strain at damage initiation and shear stress ratio (θ_s) which is defined as follows

$$\theta_s = \left(q + k_s p\right) / \tau_{\max} \tag{22}$$

where $\tau_{\max}$ is the maximum shear stress and k_s is material parameter.

3 MODEL VERIFICATION

In order to verify the proposed model, the STCC specimens tested by Nematzadeh (2012) are modeled in ABAQUS program and the results are compared with the experimental ones. Characteristics of STCC specimens along with their ID are presented in Table 2, according to the experimental research (Nematzadeh, 2012). Also, the analytical results obtained from the modeling along with the experimental results are given in Table 3. These results include the compressive strength at the steel yield stress, the initial peak strength (strength at the steel strain hardening) and the ultimate strength as well as the longitudinal to hoop stress ratio of the steel tube at the yield stress and the strain hardening. It can be seen from the table that the experimental and analytical results of the compressive strengths, especially the initial peak strength, are very close to each other, indicating a good agreement for the columns strength. Fig. 11 illustrates the experimental results of the compressive strength versus the analytical ones. As can be seen from the figure, the data points are properly distributed close to the bisector line.

According to the FE results, the mean values of longitudinal to hoop stress ratio of the steel tube at the yield stress and the strain hardening are equal to 1.3 and 2.1, respectively. These values exhibit a little difference with the experimental values, which are reported equal to 1 and 2 (Nematzadeh, 2012), respectively. Also, the axial and lateral stress-strain relationships of STCC specimens obtained from FEA are compared with the experimental results and a good agreement is

achieved, as shown in Figs. 12 and 13. A comparison between the analytically predicted failure mode and the experimentally observed one is illustrated in Fig. 14 for a typical STCC specimen (N50P650-2.5). According to the figure, the FE deformed shape at the failure point is in a good agreement with that obtained from the experimental test.

By comparing the results of finite element analysis with the experimental results for the various parameters, it can be found that the FE proposed model is able to properly predict the compressive behavior of STCC columns and calibrate the parameters required for modeling in ABAQUS program.

Specimen ID	Steel tube wall thickness (mm)	Outer diameter-to-wall thickness ratio	Specimen length (mm)	Concrete compressive strength (MPa)	Yield and ultimate strength of steel (MPa)
N25P350-2.5	2.5	24.2	140.0	28.2	339,480
N25P950-1.5	1.5	39	139.6	31.7	339,480
N25P650-1.5	1.5	39	138.9	28.3	339,480
N35P650-1.5	1.5	39	138.5	42.4	339,480
N15P650-1.5	1.5	39	139.5	20.5	339,480
N25P950-2.5	2.5	24.2	138.4	30	339,480
N50P650-2.5	2.5	24.2	140.9	50.5	339,480
N15P550-2.5	2.5	24.2	140.6	16.7	339,480
N35P550-2.5	2.5	24.2	141.2	37.1	339,480
N25P650-2.0	2	29.75	140.3	26.7	339,480
N25P500-2.5	2.5	24.2	141.8	26.7	339,480
N25P2000-1.0	1	57.5	139.2	25.8	339,480
N45P650-1.5	1.5	39	140.3	45.43	339,480
N47P650-1.5	1.5	39	140.7	46.9	339,480

*The inner diameter of steel tube is constant and equal to 55.5 mm in all specimens.

Table 2: Properties of STCC specimens (Nematzadeh, 2012).

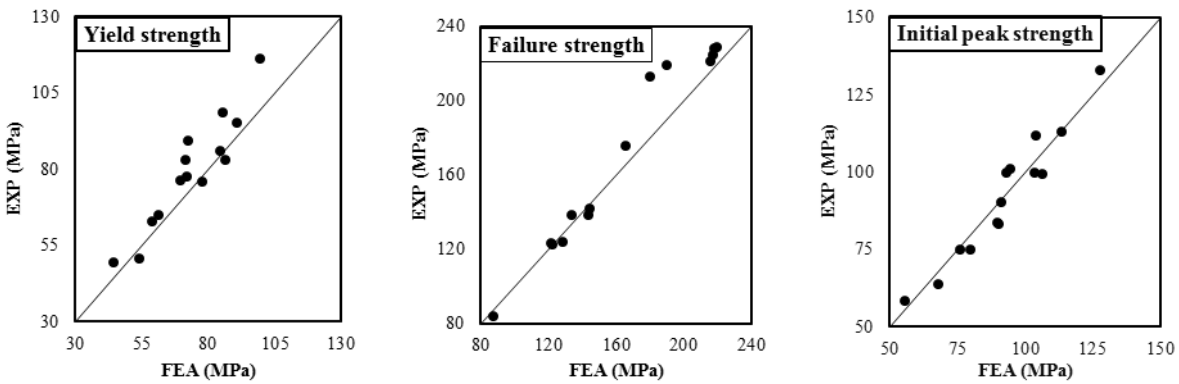

Figure 11: Relationship between experimental results of compressive strength and analytical results of STCC at the points of steel yielding, initial peak and failure.

Specimen ID	Strength corresponding to steel yielding (MPa)		EXP/FEA	Initial peak strength (MPa)		EXP/FEA	Failure strength (MPa)		EXP/FEA	Longitudinal to hoop stress ratio of steel tube	
	EXP	FEA		EXP	FEA		EXP	FEA		Yielding point	Strain hardening point
N25P350-2.5	98.6	85.4	1.15	111.6	104.3	1.07	219.4	189.9	1.15	2.27	1.46
N25P950-1.5	64.8	61.3	1.06	74.8	79.6	0.94	123.8	128.6	0.96	1.95	1.21
N25P650-1.5	62.7	58.9	1.06	75.0	76.1	0.99	138.3	134.2	1.03	1.94	1.21
N35P650-1.5	76.2	69.3	1.10	83.3	90.4	0.92	122.6	122.6	1.00	2.02	1.22
N15P650-1.5	50.7	54.2	0.94	63.7	67.9	0.94	123.1	121.5	1.01	2.01	1.33
N25P950-2.5	83.2	86.3	0.96	99.3	106.6	0.93	227.7	218.4	1.04	2.29	1.43
N50P650-2.5	116.4	99.3	1.17	132.7	127.7	1.04	221.2	215.8	1.02	2.16	1.36
N15P550-2.5	75.9	77.9	0.97	90.3	91.2	0.99	212.8	179.9	1.18	2.12	1.35
N35P550-2.5	95.3	90.8	1.05	113.0	113.7	0.99	229.0	219.8	1.04	2.23	1.49
N25P500-2.5	85.9	84.6	1.02	99.9	103.7	0.96	224.8	217.3	1.03	2.33	1.44
N25P650-2.0	77.6	71.7	1.08	83.6	89.8	0.93	175.6	165.8	1.06	2.17	1.38
N45P650-1.5	82.9	71.7	1.16	99.7	93.3	1.07	138.6	143.9	0.96	2.02	1.22
N25P2000-1.0	49.2	44.5	1.11	58.1	55.8	1.04	83.7	87.4	0.96	1.89	1.18
N47P650-1.5	89.1	72.3	1.23	101.1	94.8	1.07	141.5	144.7	0.98	1.99	1.20

Table 3: Finite element analysis results.

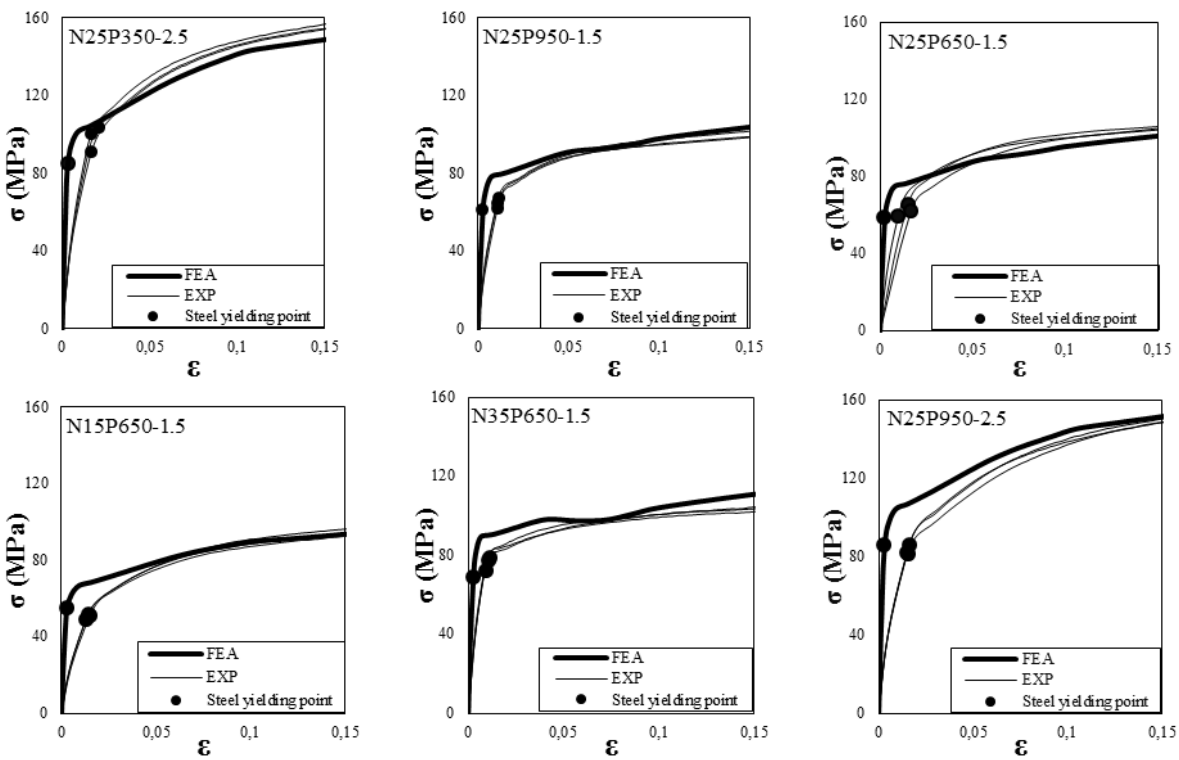

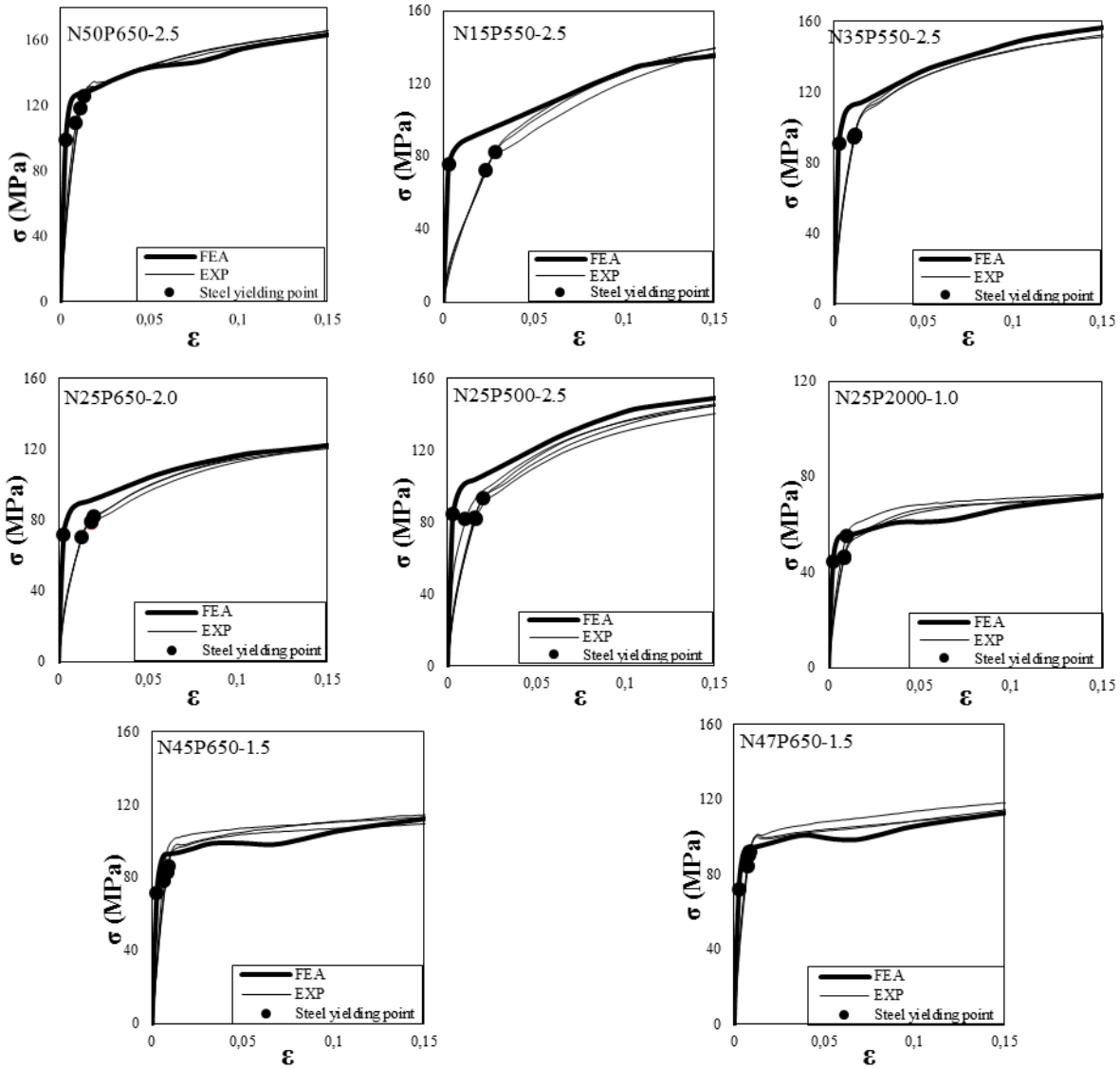

Figure 12: Axial stress-strain curves of STCC specimens.

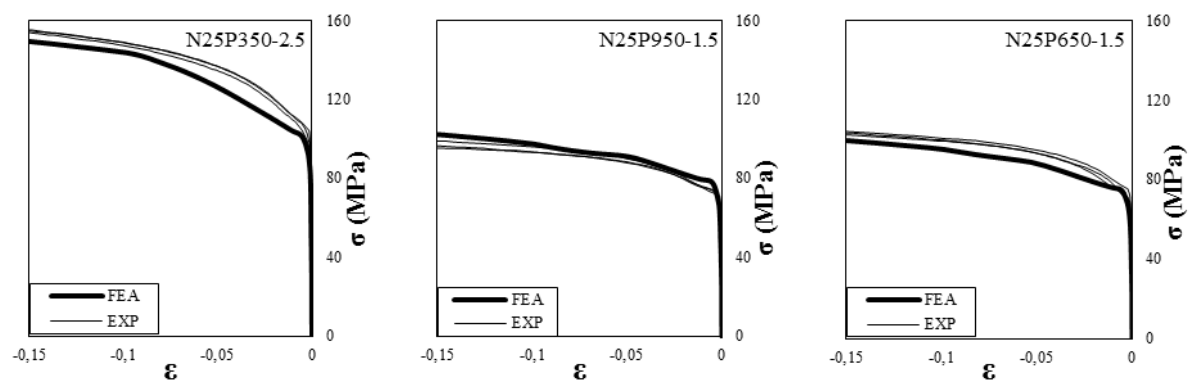

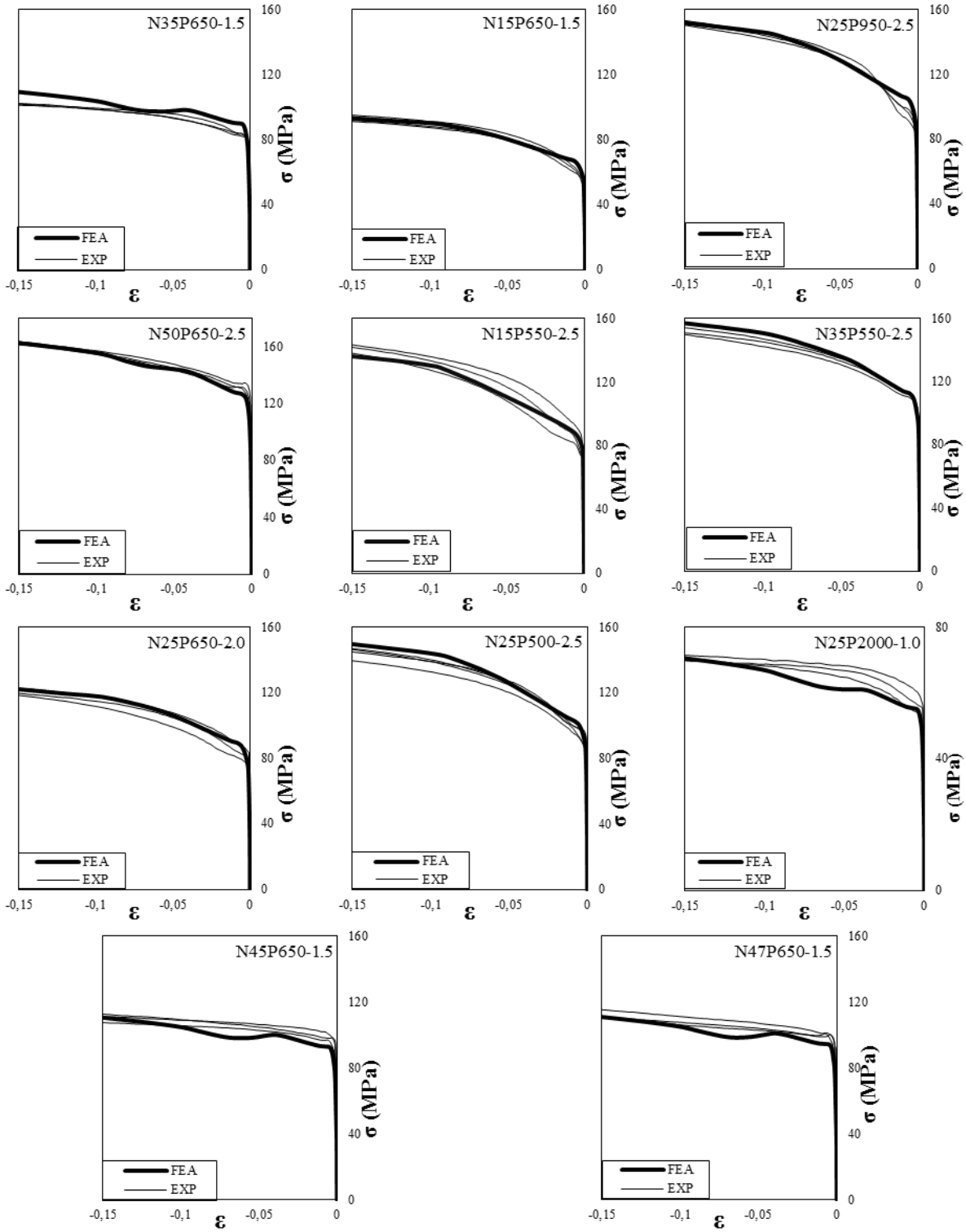

Figure 13: Lateral stress-strain curves of STCC specimens.

Figure 14: A comparison between analytically predicted and experimentally observed failure mode for a typical STCC specimen (N50P650-2.5).

4 PARAMETRIC STUDY

4.1 Specimens

By calibrating the required parameters for modeling the STCC columns in ABAQUS program, the effect of geometrical and mechanical properties of the composite section on its compressive behavior can be investigated as a parametric study. These parameters include the concrete compressive strength (f_c), tube outer diameter-to-wall thickness ratio (D/t) and steel yield stress (f_y). For this purpose, 100 specimens with 5, 5 and 4 different values of f_c, D/t and f_y, respectively, are selected the properties of which are given in Table 4.

To investigate the effect of the strain hardening stage of steel on the compressive behavior of STCC columns, bilinear and trilinear curves are used to define the equivalent stress–strain relationship of steel.

f_c (MPa)	t (mm)	D/t	f_y (MPa)	D_c (mm)	L_c (mm)	L_s (mm)
20, 30, 40, 50, 60	1, 1.2, 1.5, 2.0, 3.0	57.5, 48.3, 39.0, 29.8, 20.5	300 (bilinear), 339 (bilinear), 339 (trilinear), 400 (bilinear)	55.5	140	150

Table 4: Specimen information for parametric study.

Nomenclature of the specimens for identification is as $S_{f_c\text{-}t\text{-}f_y}$ where the characters after letter S, represent the values of concrete compressive strength, steel tube wall thickness and steel yield stress along with the type of steel stress-strain relationship as bilinear (b) or trilinear (t), respectively. For example, $S_{35\text{-}2\text{-}339b}$ represents a STCC specimen with concrete compressive strength of of 35 MPa, steel tube wall thickness of 2 mm and steel yield stress of 339 MPa with bilinear stress-strain

curve. Also, to identify a group of the specimens with constant value for one of the parameters, only the value of that parameter is replaced by the corresponding letter in specimens' nomenclature. For example, $S_{f_c\text{-}1\text{-}f_y}$ represents all STCC specimens with steel tube wall thickness of 1 mm.

4.2 Results and Discussion

After modeling the STCC specimens under axial compression load, the results obtained from finite element analysis are evaluated. These results include yield strength, initial peak strength, ultimate strength, axial stress-strain curve of composite section and its components and the interaction between concrete and steel including interface shear stress and confining pressure. As mentioned before, the point corresponding to beginning of the steel strain hardening is considered as the initial peak point. Since strain hardening in the steel with bilinear curve does not occur, the inflection point in the composite column stress-strain curve where the curve changes from concave downward to concave upward, is considered as the initial peak point. The findings of this research indicate that the difference in the stress-strain curve of STCC columns between the specimens with bilinear and trilinear steel stress-strain relationship begins from the inflection point which is corresponding to the strain hardening point of the trilinear one. The compressive strength corresponding to the initial peak point is applied to evaluate the composite section strength under small deformations. It should be noted that the ultimate strength for STCC columns with an appropriate confinement occurs at the failure point with a large axial strain, which is between 0.37 and 0.56 for the specimens of this study.

4.2.1 Composite Section Compressive Strength

The relationship of the composite section compressive strength at the steel yielding point (f_{yc}), the initial peak point (f_{cc}) and the ultimate point (f_{uc}) versus the concrete compressive strength for different values of the tube diameter-to-wall thickness ratio is illustrated in Fig. 15. The yield stress of steel tube is constant for all the specimens and is equal to 339 MPa with trilinear curve ($S_{f_c\text{-}t\text{-}339t}$).

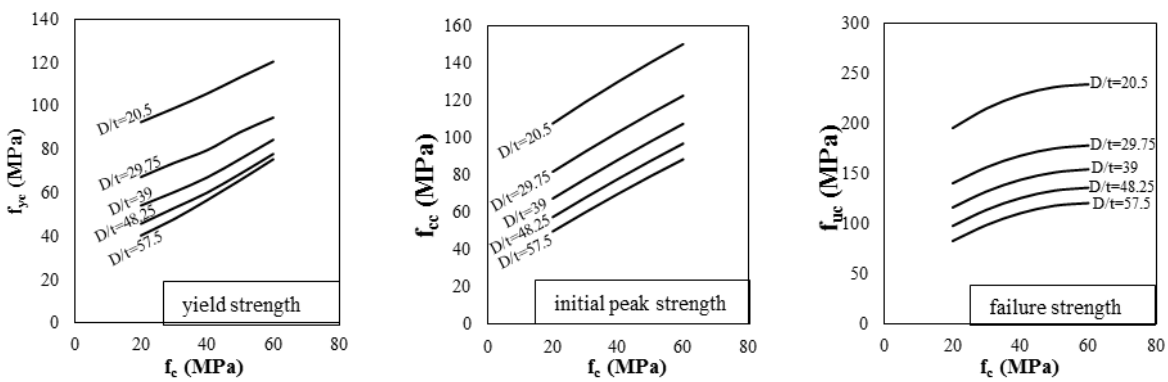

Figure 15: Relationship of compressive strength of STCC columns ($S_{f_c\text{-}t\text{-}339t}$) versus f_c at the points of steel yielding, initial peak and failure for different values of D/t.

According to the figure, with increasing the concrete compressive strength, the composite compressive strength increases so that the rate of increase in the compressive strength at the steel yielding point and the initial peak point is approximately constant and exhibits a decreasing trend at the ultimate point, which is due to a faster failure in the specimens with a higher concrete compressive strength. Hence, the effect of increasing the concrete compressive strength on the improvement of the composite failure strength significantly decreases with the increase in the concrete compressive strength. Furthermore, increasing the tube outer diameter-to-wall thickness ratio leads to a reduction in the confining pressure and thus a reduction in the composite compressive strength. This trend is more evident for lower values of the tube diameter-to-wall thickness ratio.

One of the parameters affecting the composite compressive strength is the steel yield stress, which is investigated in Fig. 16. In the study of this parameter, the wall thickness of steel tube is considered constant and equal to 1 mm ($S_{f_c\text{-}1\text{-}f_y}$). Also, the stress-strain curve of steel is bilinear with the yield stress of 300, 339 and 400 MPa in all the specimens. It can be seen from Fig. 16 that the relationship between the composite compressive strength (f_{yc}, f_{cc} and f_{uc}) and the steel yield stress is linear. Also, the parallel lines in Fig. 16 demonstrate that the trend of changes in the composite compressive strength versus the steel yield stress for different values of the concrete compressive strength is the same. In addition, it can be concluded from the equal distances between the composite compressive strength curves at the steel yielding point and the initial peak point that there is a linear relationship between the composite compressive strength and the concrete compressive strength, as demonstrated earlier. This trend for the composite failure strength is associated with a reduction in the distance between the curves as the concrete compressive strength increases, which is caused by a faster failure in the specimens with a higher concrete compressive strength because of a higher brittleness.

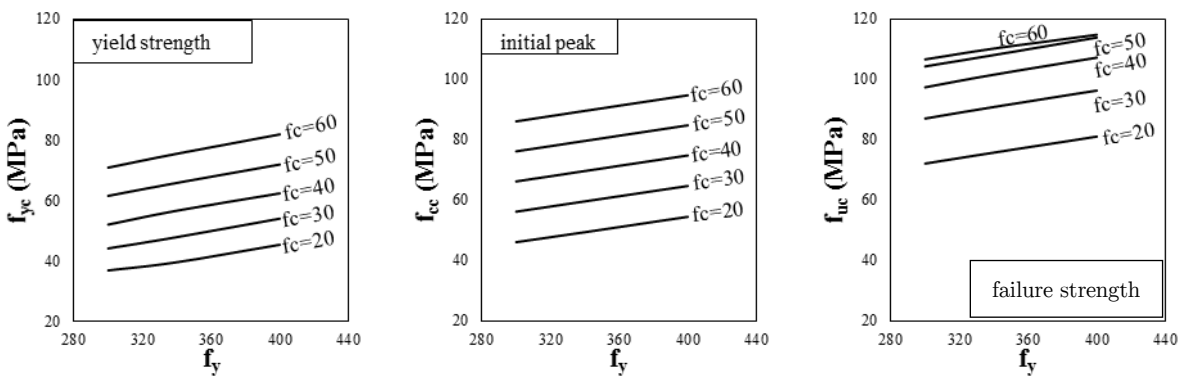

Figure 16: Relationship of compressive strength of STCC columns ($S_{f_c\text{-}1\text{-}f_y}$) versus f_y at the points of steel yielding, initial peak and failure for different values of f_c.

4.2 .2 Interface Shear Stress

Shear stress distribution of STCC specimens in the concrete core height due to the friction at the concrete–steel interface at the points of steel yielding, initial peak and failure is shown in Fig. 17. In

order to study this parameter, the results of two groups of specimens including $S_{f_c\text{-}1\text{-}339t}$ and $S_{f_c\text{-}3\text{-}339t}$ are evaluated. It can be seen from Fig. 17 that the shear stress distribution in the height direction is non-uniform so that its value is maximum at the two ends and is zero at the mid-height of the specimens due to the symmetry.

It can also be found from Fig. 17 that the shear stress between the concrete core and steel tube at the points of steel yielding and initial peak is not influenced by the concrete compressive strength while with increasing the steel tube wall thickness, the interface shear stress increases significantly. This is due to the fact that with increasing the tube wall thickness, the confining pressure and consequently the friction stress at the interface increase while increasing the concrete compressive strength has a negligible effect on it. At the failure point, the sign of shear stress changes around both ends of the specimens. Since there is a large deformation of STCC specimens at the failure point, the end parts of concrete core tend to contract and due to the end restraints, an outward shear stress is created at both ends.

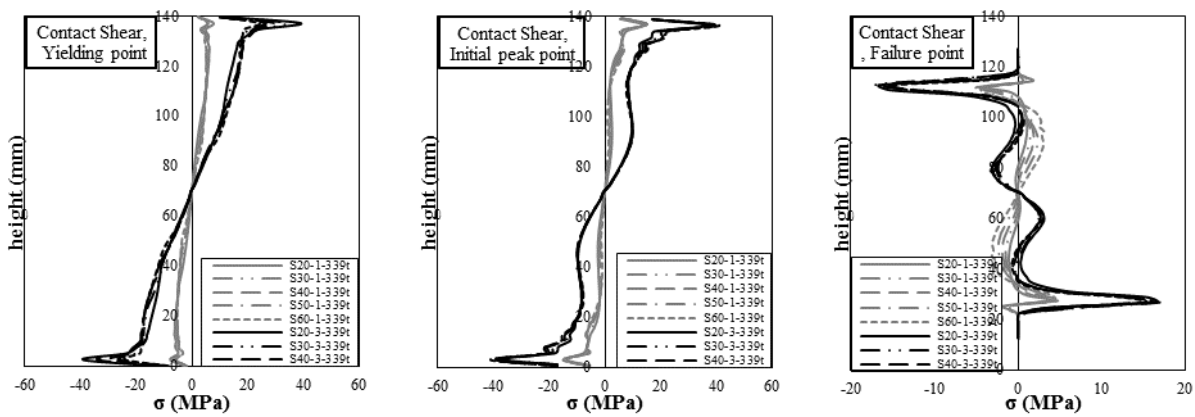

Figure 17: Interface shear stress along concrete height at the points of steel yielding, initial peak and failure.

4.2.3 Lateral Confining Pressure

Fig. 18 shows the confining pressure distribution in the height of concrete core at the points of steel yielding, initial peak and failure. In order to study this parameter, the results of two groups of the specimens including $S_{f_c\text{-}1\text{-}339t}$ and $S_{f_c\text{-}3\text{-}339t}$ are evaluated. It can be found from the figure that in all the specimens, the maximum lateral pressure occurs at the two ends of the specimens and the minimum one is created at the mid-height. Since the lateral deformation of the specimens at the ends is completely prevented, a significant pressure is applied on the concrete core while the end effects are insignificant in the middle of the specimens, and the lateral strains are only restrained by the steel tube. Therefore, the confining pressure at the mid-height of the specimens is minimum. According to the results of this research, longitudinal stress of the steel tube at the mid-height of the specimens is maximum. Hence, based on the von Mises yield criterion and isotropic hardening model, the circumferential tensile stress and consequently the confining pressure at the mid-height of the steel tube are lower than those at other points of the height.

It can also be seen from Fig. 18 that the increase in the concrete compressive strength has an insignificant effect on the confining pressure of the STCC specimens at the points of steel yielding, initial peak and failure. This fact can be proved using the equation $f_l = \frac{2 f_y t}{D - 2t}$ derived from the classical elasticity theory, in which the lateral confining pressure (f_l) is independent of the concrete compressive strength. Moreover, the lateral confining pressure obtained in Eq. (4) is only a function of the geometrical and mechanical properties of steel tube. It can be also found from Fig. 18 that with increasing the tube wall thickness, the lateral confining pressure significantly increases over the height of STCC specimens.

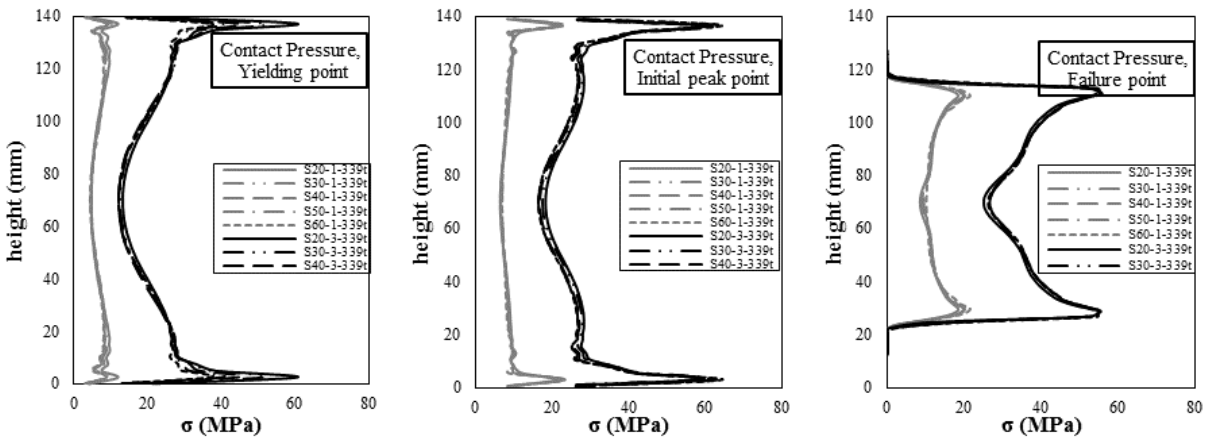

Figure 18: Confining pressure along concrete height at the points of steel yielding, initial peak and failure.

4.2 .4 Load -Carrying Capacity

Load-carrying capacity of steel tube and concrete core during the loading for $S_{f_c\text{-}1\text{-}339t}$ and $S_{f_c\text{-}3\text{-}339t}$ specimens is shown in Fig. 19, which is obtained at the mid-height of the STCC specimens. It can be seen from the figure that with increasing the concrete compressive strength, load carrying portion of concrete core increases while that of steel tube is changed insignificantly. Also, with increasing the axial load in large deformations, load carrying portion of concrete core increases while that of steel tube decreases. The reason is that the lateral pressure applied on the inner wall of the steel tube in large lateral deformations leads to a significant reduction in the longitudinal compressive stress of steel tube and its load-carrying portion and consequently an increase in the load-carrying portion of concrete core. It should be noted that the vertical component of the confining pressure is in the opposite direction of the interface shear stress vertical component.

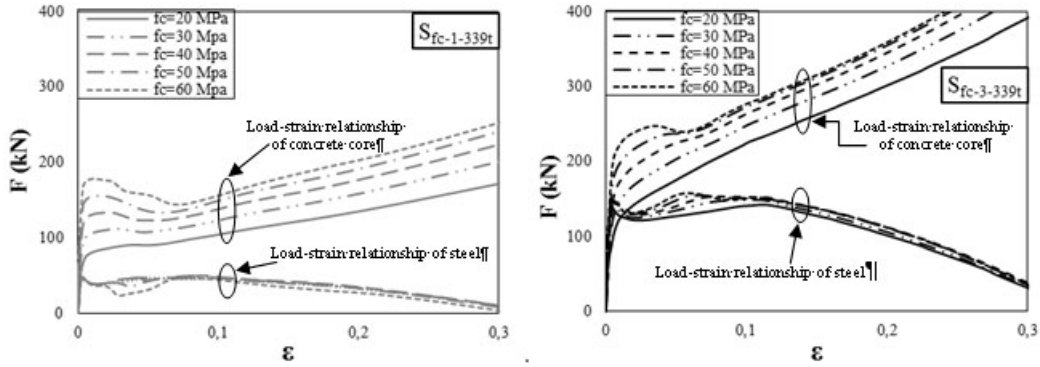

Figure 19: Load carrying portion of concrete core and steel tube in STCC columns for different values of f_c.

4.2.5 Volumetric Strain

Volumetric strain of concrete core (ε_v) can be calculated from the sum of axial and lateral strains. Normalized axial stress relationship of the STCC specimens (ratio of axial stress to stress at steel yielding point) versus volumetric strain of concrete is presented in Fig. 20. The positive and negative volumetric strains indicate the contraction and expansion of the concrete core, respectively. It can be observed from the figure that the concrete volumetric strain until the steel yielding point is independent of the concrete compressive strength and all the curves in each of the groups $S_{f_c\text{-}1\text{-}339t}$ and $S_{f_c\text{-}3\text{-}339t}$ are consistent with each other. Nonetheless, the concrete volumetric strain is significantly affected by the steel tube wall thickness. It can be found from the figure that in all the specimens, the maximum contraction volumetric strain occurs near the steel yielding point. Also, the zero volumetric strain, where the volumetric strain changes from the contraction to the expansion condition, happens shortly after the steel yielding point and before the initial peak point so that with increasing the concrete compressive strength and the steel tube wall thickness, the normalized stress corresponding to the zero volumetric strain increases.

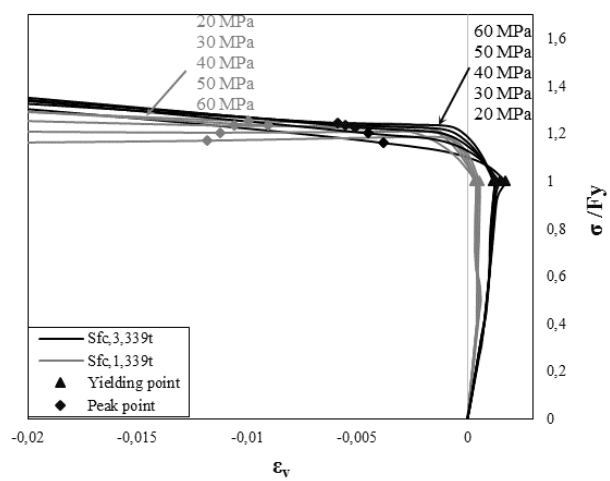

Figure 20: Normalized axial stress of composite column versus volumetric strain of concrete core.

4.2 .6 Axial Stress Contour

Distribution of the axial stress on the concrete core cross-section of STCC specimens at the point of steel yielding is illustrated in Fig. 21. Considering that the maximum and minimum values of the interface shear stress take place at the two ends and the mid-height of the STCC specimens, respectively, the stress distribution given in the figure is obtained for a section in the middle of the end and mid-height of the concrete core. It can be found from the figure that the axial stress in the concrete cross-section is uniformly distributed at the steel yielding point. Also, with increasing the distance from the concrete core center, the value of axial stress is reduced gradually so that the minimum one occurs in the extreme layer of the concrete core. The reason is that the effect of interface shear stress on the axial stress of concrete core is reduced with decreasing the distance from the core center.

Based on the comparison between stress contours of $S_{60\text{-}1\text{-}339t}$ and $S_{60\text{-}3\text{-}339t}$ specimens in Fig. 21, it can be concluded that with a constant value of the concrete compressive strength, increasing the steel tube wall thickness leads to an increase in the stress factors and as a result an increase in concrete axial stress values. Furthermore, the stress distribution in $S_{60\text{-}1\text{-}339t}$ specimen is more uniform than that of $S_{60\text{-}3\text{-}339t}$ one. This indicates that with increasing the tube wall thickness, the stress distribution in the concrete cross-section becomes more non-uniform. The reason of this trend is that with increasing the tube wall thickness, the load carrying portion of the steel tube and consequently the interface shear stress increase, resulting in an increase in non-uniformity of the axial stress of concrete core in the radial direction. From the comparison between stress contours of $S_{20\text{-}3\text{-}339t}$ and $S_{60\text{-}3\text{-}339t}$ specimens in Fig. 21, it can be found that increasing the concrete compressive strength leads to a reduction in the stress factors, however, the axial stress values are increased. In addition, the stress distribution of $S_{60\text{-}3\text{-}339t}$ specimen at the points of steel yielding and initial peak is more uniform than that of $S_{20\text{-}3\text{-}339t}$ one. This indicates that with increasing the concrete compressive strength, the stress distribution of composite section is more uniform. However, this trend is not observed at the failure point because of the large lateral deformations.

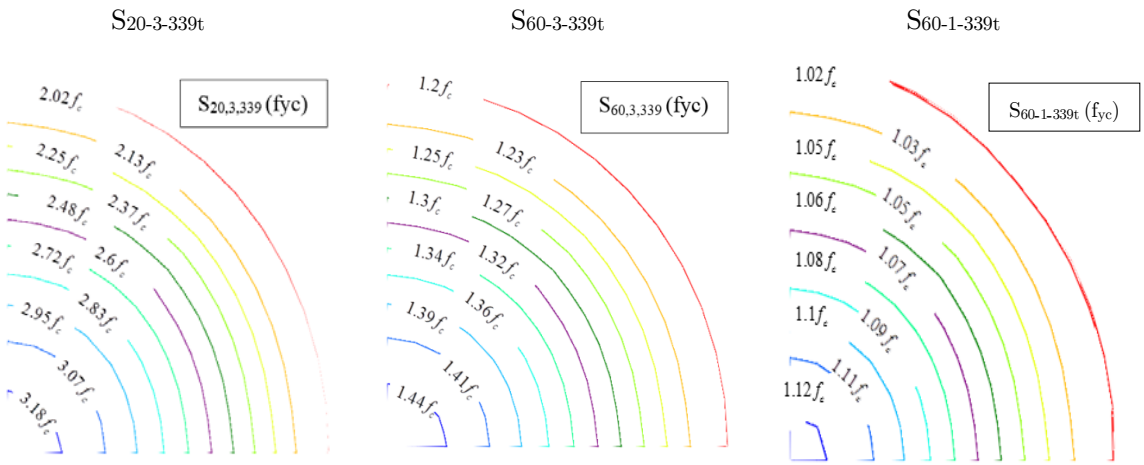

Figure 21: Axial stress distribution on concrete core cross-section at the points of steel yielding.

5 CONCLUSIONS

This research presented a nonlinear finite element analysis of axially loaded STCC stub columns with confinement effect. Quantitative and qualitative verifications performed in this study indicate that the FE proposed model can well predict the compressive behavior of STCC columns and calibrate the parameters required for the modeling in ABAQUS program. Based on the numerical results, the following conclusions may be drawn:

1. The extended Drucker-Prager model is used for the concrete yield surface, in which the flow stress ratio (K), friction angle (β) and cohesion parameter (d) are obtained as 0.8, 20° and 0.88, respectively, by matching the numerical results with experimental data via trial and error. A non-associated flow rule is used to define the direction of the plastic flow, in which volumetric dilation angle ψ is obtained as 35°.
2. The lateral confining pressure (f_l) to define the concrete material was achieved independent of f_c, which decreases with an increase in D/t. Also, the final stress parameter K' decreases with increasing f_c and D/t due to the low concrete ductility and the lateral confinement, respectively.
3. The load-carrying capacity of the STCC specimens is enhanced by increasing f_c and f_y. Also, with increasing f_c, load carrying portion of concrete core increases while that of steel tube is changed insignificantly.
4. The distribution of the interface shear stress and lateral confining pressure is non-uniform in the height direction of the STCC specimens so that the maximum and minimum values occur at the two ends and the mid-height, respectively. Also, none of them are influenced by f_c while significantly increase with decreasing D/t.
5. For all the STCC specimens, the maximum contraction volumetric strain occurs near the steel yielding point. Also, the zero volumetric strain happens shortly after the steel yielding point and before the initial peak point.
6. With increasing the distance from the concrete core centerline, the axial stress value in the concrete cross-section is reduced gradually so that the minimum value occurs in the extreme layer. The increase D/t of and f_c results in a more uniform distribution of axial stress in the concrete cross-section.

References

ABAQUS 6.12 Documentation, ABAQUS Users and Analysis Users Manual 2012, Providence R.I.

Aboutaha, R.S. and Machado, R. (1998). Seismic resistance of steel confined reinforced concrete (SCRC) columns. Struct Design Tall Build 7(3):251–260.

ACI Committee 318. (2008). Building code requirements for structural concrete and commentary. ACI 318M-08. USA: American Concrete Institute.

Bahrami, A. , Wan Badaruzzaman, W.H. and Osman S.A. (2013). Behaviour of stiffened concrete-filled steel composite (CFSC) stub columns. Latin American Journal of Solids and Structures 10(2):409-440.

Bahrami, A. , Wan Badaruzzaman, W.H. and Osman S.A. (2014). Numerical study of concrete-filled steel composite (CFSC) stub columns with steel stiffeners. Latin American Journal of Solids and Structures 11(4):409-440.

Chen, W.F. and Saleeb, A.F. (1994). Constitutive Equations for Engineering Materials. Volume 1: Elasticity and Modeling. Studies in Applied Mechanics 37.

Ellobody, E., Young, B. and Lam, D. (2006). Behaviour of normal and high strength concrete-filled compact steel tube circular stub columns. Journal of Constructional Steel Research 62(7): 706–715.

Gupta, P.K., Singh, H. (2014). Numerical study of confinement in short concrete filled steel tube columns. Latin American Journal of Solids and Structures 11(8): 1445–1462.

Han, L.H., Yao, G.H., Chen, Z.B. and Yu, Q. (2005). Experimental behaviour of steel tube confined concrete (STCC) columns. Steel and Composite Structures 5(6):459–484.

Hu, H.T. and Schnobrich, W.C. (1989). Constitutive modeling of concrete by using nonassociated plasticity. Journal of Materials in Civil Engineering 1(4):199–216.

Hu, H.T., Huang, C.S., Wu, M.H. and Wu, Y.M. (2003). Nonlinear analysis of axially loaded concrete-filled tube columns with confinement effect. Journal of Structural Engineering ASCE 129(10):1323–1329.

Huang, C.S., Yeh, Y.K., Liu, G.Y., Hu, H.T., Tsai, K.C., Weng, Y.T., Wang, S.H. and Wu, M.H. (2002). Axial Load Behavior of stiffened concrete-filled steel columns. Journal of Structural Engineering 128(9):1222–1230.

Kupfer, H., Hilsdorf, H.K. and Rusch, H. (1969). Behavior of concrete under biaxial stresses. ACI J 66:656–566.

Leckie, F.A. and Bello, D.J. (2009). Strength and stiffness of engineering systems. Technology & Engineering.

Mander, J.B., Priestley, M.J.N. and Park, R. (1988). Theoretical stress–strain model for confined concrete. Journal of Structural Engineering, ASCE 114(8):1804–1826.

Nematzadeh, M. (2012). Determining the relationships of active confinement of fresh concrete by prestressing steel tubes. Dissertation for Degree of Doctor of Philosophy, University of Mazandaran [in Persian].

Richart, F.E., Brandtzaeg, A. and Brown, R.L. (1928). A study of the failure of concrete under combined compressive stresses. Bulletin 185; Univ. of Illinois Engineering Experimental Station; Champaign 111.

Saenz, L.P. (1964). Discussion of 'Equation for the stress–strain curve of concrete' by P. Desayi, and S. Krishnan. Journal of the American Concrete Institute 61:1229–1235.

Schneider, S.P. (1988). Axially loaded concrete-filled steel tubes. Journal of Structural Engineering 124(10):1125–38.

Tomii, M., Sakino, K., Watanabe, K. and Xiao, Y. (1985). Lateral load capacity of reinforced concrete short columns confined by steel tube. In: Proceeding of International Speciality Conference on Concrete Filled Steel Tubular Structures 19–26.

Wang, W., Guo, Z. and Shi, Y. (2011). Finite Element Analysis on Behavior of the Joint with Steel Tube Confined Concrete (STCC) Column to Reinforced Concrete Beam. Advanced Materials Research 243-249:527–530.

Yu, Q., Tao, Z., Liu, W. and Chen, Z.B. (2010). Analysis and calculations of steel tube confined concrete (STCC) stub columns. Journal of Constructional Steel Research 66:53–64.

Appendix A

Shear strength ratio (K) for the confined concrete can be obtained from the ratio of shear strength in the equal biaxial compression to the shear strength in triaxial compression with the equal lateral confining pressure in such a way that the equivalent pressure stress is the same in both cases. According to the plasticity theory of extended Drucker-Prager model, the two stress conditions correspond to different circumferential points on the deviatoric plane (the former is at the lowest point of plane and the latter is at the highest one). Hence, different values of shear strength can be expected for the two cases, so that the former and latter exhibit the lowest and highest shear strength, respectively. Using the experimental results of Kupfer et al. (1969) for the concrete under an equal biaxial compression, the shear strength is 1.16 times larger than its uniaxial compressive strength. Also, to determine the

shear strength in triaxial compression with the equal lateral confining pressure, the confinement equations of STCC columns proposed by Nematzadeh (2012) are used. Finally, the shear strength ratio in the two stress conditions is achieved equal to 0.846, the calculations process of which is explained below.

Equivalent pressure stress (p') and shear strength (q') for concrete under equal biaxial compression can be achieved by Eq. (16), Eq. (17) and the results of (Kupfer et al. 1969), as follows

$$p' = 2.32 f_c / 3 \tag{A.1}$$

$$q' = 1.16 f_c \tag{A.2}$$

Based on the results of (Nematzadeh, 2012), the compressive strength of concrete core in STCC columns is equal to

$$f_{cc} = f_c + 2.17 f_l \tag{A.3}$$

Thus, equivalent pressure stress (p) and shear strength (q) for concrete under triaxial compression with equal lateral confining pressure can be obtained as follows

$$p = (f_c + 4.17 f_l) / 3 \tag{A.4}$$

$$q = f_c + 1.17 f_l \tag{A.5}$$

Equalizing the values of equivalent pressure stress in the two cases ($p = p'$) yields

$$f_l = 0.317 f_c \tag{A.6}$$

Thus, the shear strength ratio ($K = \frac{q'}{q}$) can be obtained as follows

$$K = \frac{1.16 f_c}{f_c + 1.17 \times 0.317 f_c} = 0.846 \tag{A.7}$$

Appendix B

Using Eqs. (A.4) and (A.5) for the concrete under triaxial compression and substituting them in Eq. (10) yields

$$(f_c + 1.17 f_l) - \tan\beta (f_c + 4.17 f_l) / 3 - d = 0 \tag{B.1}$$

And another form of the equation gives

$$(1 - \frac{\tan\beta}{3}) f_c - (4.17 \frac{\tan\beta}{3} - 1.17) f_l - d = 0 \tag{B.2}$$

Considering that Eq. (B.2) is true for any value of lateral confining pressure, it is necessary to establish the following equation.

$$4.17 \frac{\tan\beta}{3} - 1.17 = 0 \tag{B.3}$$

Consequently, solving the above equation yields

$$\beta = 40^\circ \tag{B.4}$$